OPEN

Varying crosslinking motifs drive the mesoscale mechanics of actin-microtubule composites

Shea N. Ricketts[1], Madison L. Francis[1], Leila Farhadi[2], Michael J. Rust[3], Moumita Das[4], Jennifer L. Ross[2] & Rae M. Robertson-Anderson[1]

The cytoskeleton precisely tunes its mechanics by altering interactions between semiflexible actin filaments, rigid microtubules, and crosslinking proteins. We use optical tweezers microrheology and confocal microscopy to characterize how varying crosslinking motifs impact the mesoscale mechanics and mobility of actin-microtubule composites. We show that, upon subtle changes in crosslinking patterns, composites can exhibit two distinct classes of force response – primarily elastic versus more viscous. For example, a composite in which actin and microtubules are crosslinked to each other but not to themselves is markedly more elastic than one in which both filaments are independently crosslinked. Notably, this distinction only emerges at mesoscopic scales in response to nonlinear forcing, whereas varying crosslinking motifs have little impact on the microscale mechanics and mobility. Our unexpected scale-dependent results not only inform the physics underlying key cytoskeleton processes and structures, but, more generally, provide valuable perspective to materials engineering endeavors focused on polymer composites.

The multifunctional mechanics of eukaryotic cells are largely determined by the cytoskeleton, a dynamic network of interacting biopolymers and binding proteins. Two principal cytoskeletal biopolymers are actin filaments and microtubules. Actin filaments polymerize from globular actin monomers to ~7 nm wide semiflexible filaments with a persistence length $l_p \approx 10\ \mu m$[1,2], while microtubules are formed by tubulin dimers polymerizing into 25 nm wide hollow rigid tubes with $l_p \approx 1\ mm$[2–6]. Networks of semiflexible actin filaments play critical roles in cell polarity and contractile and migratory processes[7,8]; while microtubules mediate intracellular trafficking and transport, chromosomal dynamics, and mitotic spindle alignment during cell division[7,9]. Synergistic interactions between these two filaments, which are mediated by steric and chemical interactions (i.e. entanglements and crosslinking)[1,8,10,11], establish essential cell asymmetries and enable proliferation, differentiation, and migration[1,8,12–14]. While crosslinking of both filaments is ubiquitous in cells, serving important roles in locomotion, membrane reinforcement, and intercellular cargo transport[4,8,14], there is mounting evidence of crosslinking *between* actin and microtubules, mediated by proteins such as tau, MAP2, APC, profilin, and plectin[8,15–21]. Specifically, actin-microtubule co-crosslinking has been shown to be important to cortical flow, wound healing, neuronal cone growth, cell migration, and muscle contraction[7–9,14,15,17,22–25].

Aside from the obvious physiological relevance, investigations of actin-microtubule composites with variable crosslinking motifs are motivated by materials engineering, as they serve as a model platform for designing and investigating flexible-stiff polymer composites[2,11,26,27]. In order to increase stiffness, strength, and toughness in composite materials, soft polymer networks are often reinforced with stiffer, load bearing fibers such as nanotubes and carbon nanofibers[11,26,28,29]. Further, varying types of crosslinking have been used to reinforce and increase the mechanical strength of flexible-stiff polymer double-networks[30–32]. Crosslinking has also been shown to preserve memory and reduce network deformation in composite polymer hydrogels[32,33].

Here, we use optical tweezers microrheology and confocal microscopy to characterize the mechanics and mobility of actin-microtubule composites with varying crosslinking motifs. We create equimolar

[1]Department of Physics and Biophysics, University of San Diego, 5998 Alcala Park, San Diego, CA, 92110, USA. [2]Department of Physics, University of Massachusetts, Amherst, 666N. Pleasant St., Amherst, MA, 01003, USA. [3]Department of Molecular Genetics and Cell Biology, University of Chicago, 900 E 57th St., Chicago, IL, 60637, USA. [4]School of Physics and Astronomy, Rochester Institute of Technology, 84 Lomb Memorial Drive, Rochester, NY, 14623, USA. Correspondence and requests for materials should be addressed to R.M.R.-A. (email: randerson@sandiego.edu)
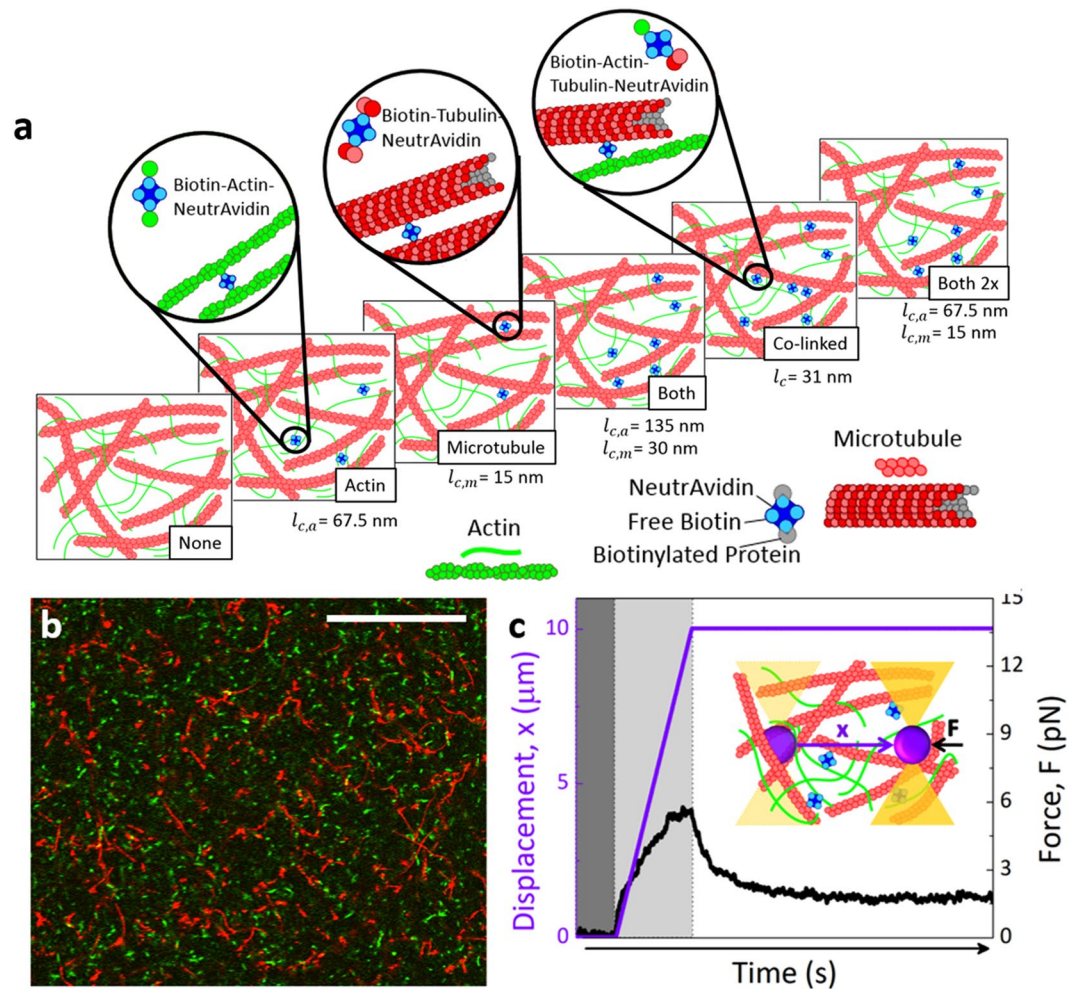
Figure 1. Schematic of experiments to probe the role that crosslinking plays in the mechanics and mobility of actin-microtubule composites. (**a**) Cartoon of molecular components comprising actin-microtubule composites with varying crosslinker motifs (*None*, *Actin*, *Microtubule*, *Both*, *Co-linked*, *Both 2x*) described in the text. The calculated length between crosslinkers for each motif is listed under each cartoon, where $l_{c,a}$ is the length between crosslinkers along an actin filament, $l_{c,m}$ is the length between crosslinkers along a microtubule, and l_c is the length between crosslinkers when actin and microtubules are linked to each other. (**b**) Two-color laser scanning confocal micrograph of 5.8 μM *Co-linked* actin-microtubule composite with ~3% of actin and microtubules labeled with Alexa-488 (green) and rhodamine (red), respectively. (**c**) Sample microrheology data for a *Co-linked* composite, showing the stage displacement (purple) and the force measured for an individual trial (black) before (dark grey region), during (light grey region) and after (white region) the stage displacement. Inset: Cartoon of optical tweezers microrheology measurement. An optically trapped 4.5 μm diameter microsphere (not drawn to scale) embedded in a crosslinked composite is displaced 10 μm (*x*, purple) at a speed of 10 μm/s while the corresponding force the composite exerts is measured (*F*, black).

composites of actin and microtubules in which: only actin is crosslinked (*Actin*), only microtubules are crosslinked (*Microtubule*), both actin and microtubules are crosslinked (*Both*), and actin and microtubules are crosslinked to each other (*Co-linked*) (Fig. 1a). We characterize mechanics by optically pulling a microsphere through the composites and simultaneously measuring the induced force during strain as well as the relaxation of force following the strain. We find that the mesoscale force response separates into two distinct classes, with one class exhibiting a substantially elastic response with minimal relaxation following strain, while the other class exhibits a softer more viscous response with nearly complete dissipation. We show that these two classes, which are only readily apparent at mesoscopic scales ($>\mu$m), are dictated by the degree to which microtubules are crosslinked.

Despite the relevance of actin-microtubule composites to biology, physics, and engineering, most *in vitro* studies to date have focused on single-component networks of either actin or microtubules[4,34–48]. In response to strain, entangled actin networks have been reported to exhibit varying degrees of stiffening, softening, and yielding depending on the actin concentration as well as the scale and rate of the strain[36,38,39]. Crosslinked actin networks exhibit enhanced stiffness and prolonged, more pronounced elasticity compared to entangled solutions[35,37,43,44]. Entangled actin networks have also been shown to relax force via an array of mechanisms including bending, stretching, retraction, reptation, and confinement-hopping[39,49–52]. While many of these mechanisms

are suppressed by crosslinking, crosslinked networks have been reported to exhibit relaxation and plasticity due to crosslinker unbinding/rebinding, slippage, and stretching[53–55]. Compared to entangled actin networks, entangled microtubules have been reported to respond more elastically to strain with more pronounced stiffening as well[4,9,42]. Further, while stretching is important to actin stress relaxation, bending plays a more dominate role in the relaxation of microtubules[56]. While the timescales for microtubules to relax have been suggested to be on the order of several minutes or more[4,42], crosslinked microtubule networks have been reported to display some degree of relaxation due to temporary force-induced crosslinker unbinding events[4].

Few studies have investigated composite networks of actin and microtubules[11,27,57,58] due, in part, to the incompatibility of standard polymerization conditions for each protein[27]. However, methods have recently been introduced to co-polymerize actin and tubulin *in situ* to create randomly-oriented co-entangled composites of actin and microtubules[27]. The first study that employed these methods used microrheology and microscopy techniques to show that a surprisingly large molar fraction of microtubules (>70%) was needed to substantially increase the response force of the composites. This intriguing result was attributed to the larger mesh size of microtubule networks compared to actin networks of the same molarity. Further, actin-rich composites softened in response to strain while microtubule-rich composites stiffened. This distinction arose from actin bending (leading to softening) that was increasingly suppressed by microtubules (leading to stiffening). This result corroborated a previous study that investigated the nonlinear macrorheology of crosslinked actin networks doped with low concentrations of microtubules, in which the high bending stiffness of microtubules served to suppress actin bending and enhance stretching in response to strain[11,43].

Results and Discussion

To systematically investigate the role that crosslinking plays in composites of actin and microtubules we design actin-microtubule composites with four distinct crosslinking motifs. We use our previously established protocols[27] to create equimolar co-entangled actin-microtubule composites. We then incorporate biotin-NeutrAvidin complexes into composites to selectively crosslink the filamentous proteins, keeping the crosslinker:protein ratio fixed at $R = 0.02$[37]. We create composites with: crosslinked actin (*Actin*), crosslinked microtubules (*Microtubule*), crosslinkers equally forming actin-actin and microtubule-microtubule bonds (*Both*), and crosslinkers binding actin to microtubules (*Co-linked*) (Fig. 1a). We compare these composites to a composite without crosslinkers (*None*) as well as one in which both filaments are crosslinked but R is doubled (*Both 2x*) (Fig. 1a). While all composites have the same crosslinker density R and protein concentration, the length between crosslinkers along actin filaments $l_{c,a}$, along microtubules $l_{c,m}$, and along both filaments l_c (for *Co-linked*) vary for the different composites, as listed in Fig. 1a and described in Methods.

Mechanical response. To characterize the mechanical response of our designed composites we use optical tweezers microrheology to drag microspheres through each composite and measure the local force applied to each sphere by the composite during and following the strain. Figure 2a shows the measured force, $F(x)$, as a microsphere is pulled through each type of composite. As expected, all crosslinked composites exhibit overall larger resistive forces than the composite with no crosslinkers (*None*). The more interesting and unexpected result that emerges is that the force curves appear to display two distinct responses dependent on the crosslinking motif: pronounced softening behavior in which the slope of the force curves approach zero at large distances, versus largely elastic behavior in which $F(x)$ remains linear with x until the end of the strain. To better delineate between these two behaviors, we normalize $F(x)$ by the terminal force F_t reached when $x = 10\,\mu$m, which we notate as $\widetilde{F}(x)$. As shown in Fig. 2b, $\widetilde{F}(x)$ distinctly separates into two classes: Class 1 comprises *None*, *Actin*, and *Both* composites while Class 2 comprises *Microtubule*, *Co-linked*, and *Both 2x* composites.

For a purely elastic material we expect to see a linear relationship between the resistive force and distance the microsphere is pulled ($F \sim x$), and once the microsphere stops the force the network exerts on the sphere $F(t)$ should be maintained with no relaxation or dissipation (i.e. mechano-memory, $F(t) \sim F_t$). Conversely, a purely viscous material yields a strain-independent force response ($F \sim x^0$) that is reached as soon as the microsphere reaches constant speed, and once the microsphere stops the network immediately and completely relaxes its force on the sphere ($F(t) \sim 0$). Most biopolymer networks, including entangled actin-microtubule composites, display viscoelastic behavior in between these two extremes[2,27]. However, crosslinking can lead to more elastic response by suppressing network rearrangements and polymer bending modes that can dissipate stress[11,37]. Figure 2b shows that Class 2 composites exhibit primarily elastic response while Class 1 exhibits softening and yielding to viscous behavior. The distinction between the two classes appears to be the degree to which microtubules are crosslinked, which we elaborate on further below.

Only composites in which microtubules are crosslinked (*Microtubule*, *Co-linked*, *Both 2x*) exhibit substantial elasticity, while *Actin* and *None* force curves display similar curvature indicative of more viscous response. This result suggests that at this crosslinking density, crosslinks do not substantially prevent semiflexible actin filaments from bending and/or rearranging to dissipate stress. Further, at a given R the length between crosslinks along an actin filament is ~4x longer than that for microtubules (see Methods), so there are comparatively fewer crosslinks along an actin filament to suppress relaxation modes. The counterintuitive result presented in Fig. 2 is that a composite in which both filaments are crosslinked (*Both*) exhibits soft/viscous behavior similar to *None* and *Actin* despite the fact that both actin and microtubules are crosslinked. Given the role that crosslinking plays in enhancing elasticity, one would expect that a network in which all filaments are crosslinked would be more elastic than one in which just half of the proteins are linked (*Actin* or *Microtubule*). However, because in this composite both actin and microtubules are crosslinked and the density of crosslinkers remains fixed ($R = 0.02$), the length between crosslinkers along each filament is doubled.

To determine if this increased $l_{c,m}$ and $l_{c,a}$ is indeed the reason for more viscous behavior for *Both* composites, we perform experiments in which we double the crosslinker density (*Both 2x*) such that the length between
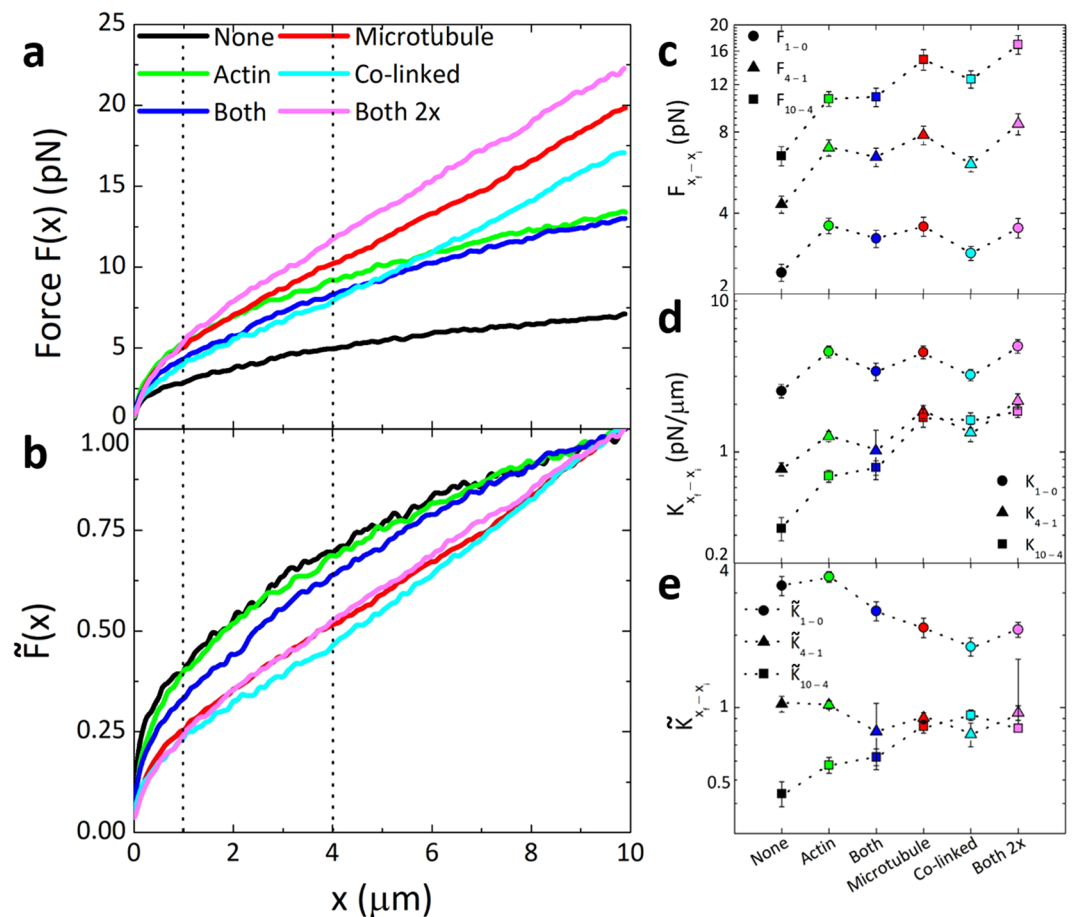
Figure 2. Mesoscale force response of crosslinked actin-microtubule composites display two distinct classes of behavior mediated by the degree of microtubule crosslinking. (**a**) Force $F(x)$ that composites with varying crosslinking motifs (listed in legend) exert to resist the $10\,\mu$m strain. Dotted vertical lines separate the different regions over which $F(x)$ and the stiffness K are averaged in (**c–e**). (**b**) The force shown in (**a**), normalized by the terminal force F_t reached at the end of the strain, denoted as $\widetilde{F}(x)$. As shown, composites separate into two distinct classes – those that exhibit substantial softening and yielding (Class 1: *None*, *Actin*, *Both*) versus those that exhibit nearly complete elastic response (Class 2: *Microtubule*, *Co-linked*, *Both 2x*). (**c**) Force values from (**a**), averaged over different bead displacements x_f-x_i, denoted as F_{xf-xi} (color coded as in (**a**)). Data shown is for x_f-$x_i = 1$–$0\,\mu$m (circles), 4–$1\,\mu$m (triangles) and 10–$4\,\mu$m (squares). (**d**) Stiffness, $K = dF/dx$, averaged over the same displacements as in (**c**), as listed in the legend. (**e**) The dimensionless stiffness, $\widetilde{K}(x) = (10\,\mu$m$)\,d\widetilde{F}(x)/dx$, averaged over the same displacements as in (**c**). Error bars in (**c–e**) are calculated from computing the standard error of force and stiffness values measured for each individual trial (~50–60 trials per data point).

crosslinkers along each actin filament and microtubule is the same as in *Actin* and *Microtubule* composites, rather than being twice as long. As shown in Fig. 2, upon doubling R, the composite exhibits Class 2 elastic-like response similar to *Microtubule* and *Co-linked* networks. Thus, it appears that the critical requirement for sustained elasticity is not only that microtubules must be crosslinked but that they must be crosslinked such that the length between crosslinkers is sufficiently small. Reducing $l_{c,m}$ leads to a more connected network, thereby constraining filament fluctuations and rearrangements and leading to enhanced network stiffness[59].

To quantify the distinct behaviors of Class 1 and Class 2 composites and examine the lengthscale dependence of the response, we average $F(x)$ over different microsphere displacements $x_f - x_i$, which we denote as F_{xf-xi} (Fig. 2c). As shown, at submicron distances on the order of the mesh size (0–$1\,\mu$m) there is little difference between the force response the two classes exhibit, with all crosslinked composites displaying an average force of $F_{1-0} \approx 3 \pm 0.6$ pN. This result indicates that variations in the crosslinking motif has little effect on the microscale, linear regime response of composites. Even at somewhat larger microscale displacements (1–$4\,\mu$m), while crosslinked composites exhibit larger forces than *None*, the type of crosslinking has little effect on the measured force (with all values lying within ~1 pN of each other). Only at mesoscale distances, on the order of the length of filaments and substantially larger than the mesh size of composites, does the dramatic effect of crosslinking motif emerge, with Class 1 composites exhibiting an average force of $F_{10-4} \approx 9 \pm 3$ pN while Class 2 composites display $F_{10-4} \approx 15 \pm 2$ pN.

This scale-dependent variation is likely a result of both variable length between crosslinkers and a small fraction of crosslinker unlinking/relinking events. At the submicron level, the differences in crosslinker lengths only

result in small differences in the density of crosslinkers encountered by the microsphere, and filament bending and stretching is minimal. As the distance becomes orders of magnitude larger than the crosslinker lengths, the effect of varying crosslinking densities, as well as the varying contributions of bending and stretching, become more appreciable. Further, at larger displacements (i.e. longer times), crosslinks that were initially ruptured (contributing to submicron softening) will have had time to re-link. While new un-linking events can occur, the force response at lengthscales much greater than l_c reflects that of a steady-state unbinding/rebinding regime, and the response will still be dominated by stretching and/or bending modes. The varying degree to which Class 1 and Class 2 composites can undergo each mode manifests as a clear distinction between measured force values at these lengthscales.

The mechanisms described above would more clearly contribute to differences in the elasticity or stiffness of the networks rather than the absolute magnitudes of the force responses. In fact, as shown in Fig. 2b, the clear distinction between Class 1 and Class 2 is in the lengthscale-dependent curvature, which quantifies the elasticity, rather than the magnitudes of the force response. To better quantify this distinct behavior, we calculate the stiffness K of composites, analogous to the differential modulus in bulk rheology, which we quantify as $K = dF/dx$ (Fig. 2d). We also compute the dimensionless stiffness $\widetilde{K}(x) = (10\,\mu m)\,d\widetilde{F}(x)/dx$, which quantifies the curvature displayed in Fig. 2b,c. Larger K and $\widetilde{K}$ values are indicative of stiffer, more elastic networks while softer more viscous behavior results in smaller K and $\widetilde{K}$ values.

As shown in Fig. 2, both classes exhibit similar K values for submicron scales, and exhibit softening (decreasing K) from K_{1-0} to K_{4-1}. Class 1 composites do soften slightly more than Class 2 composites over the first $4\,\mu m$; however, the differing degrees of softening for Class 1 and Class 2 composites is much more substantial at larger lengthscales ($>4\,\mu m$). K_{10-4} values drop to $\sim0.6 \pm 0.2$ pN/μm for Class 1 composites, whereas for Class 2 composites K_{10-4} values are indistinguishable from K_{4-1} values (no softening). To better quantify the extent to which composites soften or remain elastic, we turn to $\widetilde{K}(x)$. As shown, $\widetilde{K}(x)$ values for Class 1 composites drop by $\sim30\%$ from ($1-4\,\mu m$) to ($4-10\,\mu m$) while Class 2 composites remain nearly constant for lengthscales beyond $1\,\mu m$.

We note that the exact choice of $1\,\mu m$ and $4\,\mu m$ to delineate different phases of the response was motivated by visually apparent changes in the curvature of the force response as seen in Fig. 2a. However, small changes to these cutoffs did not alter the data presented in Fig. 2c–e in a statistically significant way. Further, to determine if the strain rate impacts these natural crossover values we repeated measurements using speeds of $2.5–20\,\mu m/s$. As shown in Fig S2, the variation between ($0–1\,\mu m$) and ($1–4\,\mu m$), as well as the magnitudes of averaged K and $\widetilde{K}(x)$ values, are similar for all speeds.

Our results and interpretations are validated by prior measurements on actin networks crosslinked by biotin-NeutrAvidin[37]. In this previous work, authors found that $R > 0.05$ was needed for actin networks to exhibit largely elastic response, with $R < 0.05$ networks displaying softening and yielding to a viscous regime over a $10\,\mu m$ bead displacement of comparable speed. The authors explained the transition to elastic response as arising from actin filaments stretching in the direction of the strain rather than bending non-affinely. This study also showed that force-induced crosslinker unbinding contributed to the yielding and relaxation behavior of low R networks. Such force-induced unbinding of biotin-NeutrAvidin crosslinkers has also previously been reported for crosslinked microtubule networks[4].

Further, our results differ from previous actin studies in which the onset of elastic response was nearly immediate. Here, our Class 2 composites display softening behavior, similar to that of Class 1 until $\sim2\,\mu m$ at which point a more elastic response takes over. This universal softening at small scales supports the presence of force-induced unbinding of both actin and microtubule crosslinks, as the length between crosslinkers is substantially smaller than a micron for all composites, whereas the deformation lengthscales needed to induce appreciable bending or stretching are much larger[35,37,60]. As the strain proceeds, the contributions from bending and stretching grow, outweighing that of crosslinker-unbinding and thus minimizing its effect on the force response. Further, unbinding events are reversible, and re-binding has been shown to contribute to sustained elastic response (coupled with partial dissipation) similar to that depicted by Class 2 composites (Fig. 2c–e)[4,35,37,60–62].

Finally, we note that the microscale response ($0–1\,\mu m$) may not solely be due to the force the composites exert but also to transient effects arising from bringing the piezoelectric stage (which moves the trapped bead) from rest to constant speed. While the response time of the stage is 0.25 ms (and accounted for in our analysis as described in Methods), the mismatch between the stage and bead velocity persists for ~25 ms (Fig S1). To test the impact of this effect on our results, we also compute the microscale quantities (F_{1-0}, K_{1-0}, $\widetilde{K}_{1-0}$) starting at 25 ms instead of 0 s. As shown (Fig S1), removing this initial period shifts the values slightly but does not change the general features or trends in the data. Further, while F_{1-0} and F_{4-1} show a weak dependence on speed (Fig S2), likely arising from this transient effect, it is much weaker than Stokes dependence ($F \sim v$) and the variation between ($0–1\,\mu m$) and ($1–4\,\mu m$) remains nearly constant.

Nonetheless, to remove transient effects entirely from the microscale analysis, we perform $1\,\mu m$ oscillatory strain measurements for frequencies $\omega = 1.26–126$ rad/s, from which we compute the frequency-dependent complex viscosity $\eta(\omega)$ (details provided in Methods). Both the magnitude and frequency dependence of $\eta(\omega)$ are nearly the same for all crosslinked composites, corroborating the microscale results described above. Further, the shear-thinning behavior $\eta(\omega) \sim \omega^{-0.5}$ is indicative of a viscoelastic fluid and is comparable to previously reported scaling for entangled actin[48], indicating once again that the elastic response of Class 2 composites only manifests at the mesoscale.

Relaxation dynamics. As described above, elastic and viscous systems should display starkly different relaxation behaviors following strain, with purely elastic systems exhibiting no relaxation and viscous systems exhibiting immediate and complete force relaxation. Viscoelastic systems display behavior in between these two extremes, with viscoelastic biopolymer networks exhibiting both exponential and power-law relaxation
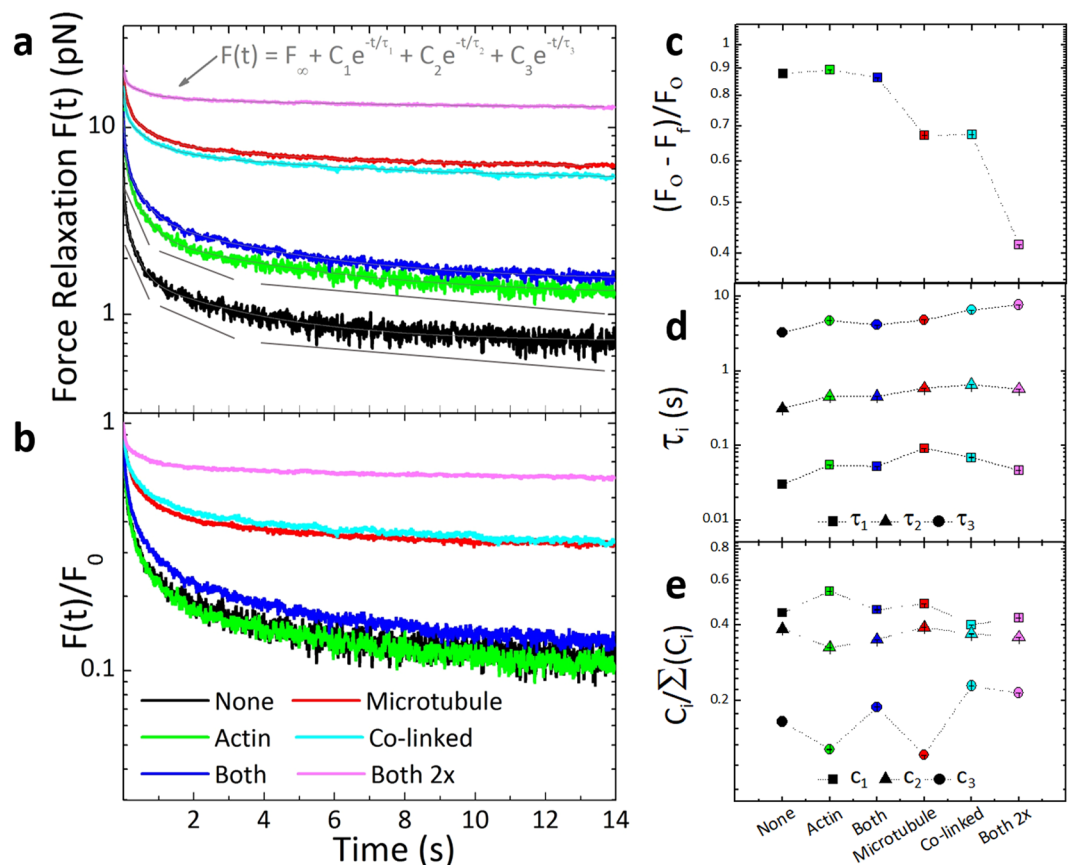
Figure 3. Actin-microtubule composites display multi-mode force relaxation with varying degrees of elasticity tuned by the crosslinker motif. (**a**) Force relaxation after microsphere displacement as a function of time $F(t)$ on a log-y scale for composites with varying crosslinking motifs listed in the legend in (**b**). Thin grey curves correspond to fits of each relaxation to the exponential sum equation displayed. Thicker grey lines guide the eye to show three distinct phases with different exponential decays (i.e different slopes). (**b**) $F(t)$ normalized by the force at the beginning of relaxation, F_o. (**c**) The fractional force dissipation, computed as $(F_o\text{-}F_f)/F_o$ where F_f is the force at the end of the relaxation measurement period. As shown, Class 1 composites exhibit much more force relaxation compared to Class 2 composites that retain substantial memory of imposed strain. (**d**) Relaxation times, τ_1 (squares), τ_2 (triangles), and τ_3 (circles) determined from the fits shown in (**a**). (**e**) Relative relaxation coefficients $C_i/(C_1 + C_2 + C_3)$ for each exponential term ($i = 1,2,3$) determined from the fits to the data (shown in (**a**)). Error bars determined from fits are shown but are smaller than the size of the symbols in most cases.

over varying timescales[2,27,36–38,63]. To characterize the relaxation dynamics of the composites, we measure the time-dependent force $F(t)$ exerted on the bead by each composite for 15 s following the strain (Figs 1, 3).

As shown in Fig. 3a, all composites exhibit some degree of force relaxation, though the extent to which the force decays depends on the crosslinking motif. This dependence becomes distinctly apparent upon normalizing $F(t)$ by the initial force (immediately after strain) F_0 (Fig. 3b). Class 1 composites exhibit faster and more complete relaxation than Class 2 composites which retain a substantial fraction of the initial force at the end of the measurement period. To quantify the varying degrees to which composites retain initial force, indicative of elastic behavior, we evaluate the fractional force dissipation $(F_o\text{–}F_f)/F_o$, in which F_f is the force reached at the end of the relaxation period. For reference, in a purely elastic network with no dissipation $(F_o\text{–}F_f)/F_o$ should be 0 whereas a viscous system should exhibit a value close to 1. As shown in Fig. 3c, a clear difference between Class 1 and Class 2 composites emerges once again. Class 1 composites dissipate ~89% of initial force whereas Class 2 composites dissipate ~40–68% of the initial force.

To determine the macromolecular mechanisms underlying the observed relaxation behavior, we evaluate fits of the force curves to a range of exponential and power-law functions that have been previously used to fit relaxation data for entangled and crosslinked biopolymer networks[27,36–38,48]. In particular, crosslinked actin networks have been shown to relax via a sum of exponential decays with well-separated decay times each corresponding to different relaxation mechanisms[37]. Similarly, we find that the best fit to the force relaxations for all composites is a sum of three exponential decays with well-separated time constants (Fig. 3a). As described below, the agreement between the measured time constants with theoretically predicted relaxation times corroborates the choice of fits to describe the data. The function used for all composites, $F(t) = F_\infty + C_1 e^{-t/\tau_1} + C_2 e^{-t/\tau_2} + C_3 e^{-t/\tau_3}$, includes an offset F_∞ that is a measure of the amount of force that the composite retains indefinitely ($F_\infty \sim F_0$ and 0 for elastic

and viscous systems respectively). The three distinct decay constants, with similar values for all composites, indicate that three different relaxation mechanisms with well-separated characteristic timescales contribute to the force relaxation of all composite types (Fig. 3d). The decay times, averaged over all composite types, are $\tau_1 = 0.06 \pm 0.02$ s, $\tau_2 = 0.51 \pm 0.12$ s and $\tau_3 = 5.28 \pm 1.83$ s. However, we note that all three timescales are ~2x faster for the unlinked composite (*None*) compared to the crosslinked composites, which we discuss further in the next section. To evaluate the relative contribution of each mechanism to the force relaxation, we compare the corresponding fractional coefficients for each exponential term $C_i/(C_1 + C_2 + C_3)$ ($i = 1,2,3$) (Fig. 3e). For all composites, the fast timescale contributes the most to the relaxation, followed by the intermediate timescale, and finally the slowest timescale. However, Class 1 composites exhibit higher C_1 values and lower C_3 values than Class 2 composites, indicating that the slowest relaxation mechanism plays a more prominent role in the relaxation of Class 2 versus Class 1 composites.

To understand our fast relaxation timescale, we estimate the fastest predicted relaxation mode for entangled actin networks, which is termed the mesh time τ_{mesh} and can be thought of as the time for hydrodynamic effects to become important (i.e. for each filament to "feel" its neighbors)[39,64]. The mesh time for our composites, computed via $\tau_m \approx \beta \zeta \xi^4 l_p^{-1}$ where is $\beta = 1/k_B T$, ζ is the translational friction coefficient and ξ is the composite mesh size (see Methods)[39,63,64], is ~0.086 s, which is quite close to our fast relaxation time $\tau_1 \approx 0.06$ s. Thus, we can interpret our fastest relaxation mechanism as arising from hydrodynamic effects of the surrounding mesh. This timescale relies on filaments being able to fluctuate and rearrange over lengthscales comparable to the mesh size. These fluctuations are hindered by rigid crosslinkers, so for smaller crosslinker lengths (Class 2) this relaxation mode should contribute less to the force relaxation. Indeed, the average C_1 value for Class 1 composites is larger than for Class 2.

Another key mode of stress relaxation accessible to actin filaments and, to a lesser extent, microtubules is bending[3,65]. We estimate timescales for actin and microtubule bending using $\tau_B \approx (\gamma/\kappa)[L/(3\pi/2)]^4$ where $\kappa \approx l_p k_B T$ is the bending rigidity, L is the filament length, $\gamma = (4\pi\eta/\ln(2\xi/r))$ is the perpendicular drag coefficient, η is the solvent viscosity, and r is the filament radius[3,39]. Using our measured lengths for actin and microtubules in composites ($L_a \approx 8.7\,\mu$m and $L_m \approx 18.8\,\mu$m)[27] we compute bending relaxation times of $\tau_{B,a} \approx 0.54$ s and $\tau_{B,m} \approx 0.15$ s for actin and microtubules, respectively. These timescales are in close agreement with our measured τ_2 values (~0.3–0.6 s), suggesting that the second relaxation mode in our experiments is due to bending of both actin and microtubules. However, Class 1 composites display larger τ_2 values than Class 2, with an average value of ~0.6 s which is quite close to the predicted $\tau_{B,a}$. Conversely, the average τ_2 value for Class 2 composites is ~0.4 s, lying between $\tau_{B,a}$ and $\tau_{B,m}$. This distinction suggests that while microtubules can freely bend in response to large strains when they are not crosslinked or minimally crosslinked (Class 1), when $l_{c,m}$ becomes sufficiently small (Class 2), microtubules can no longer bend to release stress. This suppression of bending modes leads to the primarily elastic response seen in Figs 2, 3.

To understand the slowest relaxation mode, which occurs on the order of ~1–10 s for all composites, we turn to previous experiments investigating the stress relaxation of crosslinked actin networks following nonlinear strain[37]. These studies reported the presence of two distinct relaxation mechanisms available to actin filaments, which both occur on similar timescales as our measured τ_3 and are both due to force-induced crosslinker unbinding and rebinding: curvilinear diffusion (reptation) and lateral confinement-hopping[37]. More specifically, crosslinked filaments can evade the confinement of the surrounding crosslinked mesh by crosslinks momentarily unlinking and thereby releasing the constraint they impose on the filaments, allowing for reptation and lateral confinement hopping. Such force-induced temporary unbinding events have been previously reported for both actin and microtubule networks crosslinked with biotin-NeutrAvidin[4,37]. Because fast timescale fluctuations (τ_1) are more suppressed in Class 2 composites, we expect this slow mode to contribute more to the relaxation of Class 2 composites compared to Class 1, which is what we see in Fig. 3e (i.e. C_3 values for Class 2 composites are largely greater than for Class 1).

Steady-state mobility. To determine the steady-state mobility of actin and microtubules in each composite type, we analyze time-series of dual-color confocal images, as described in Methods and previously validated[27]. Briefly, for each time-series we compute the average standard deviation of the intensity over time for all pixels $<\delta>$ and normalize by the corresponding average intensity of all pixels over time $<I>$ (Fig. 4). Higher values of this mobility metric indicate a more mobile network of filaments that fluctuates more while lower values imply a more static network.

Comparing $<\delta>/<I>$ values for actin and microtubules in the same composite, we find that actin filaments in all composites fluctuate significantly more than microtubules with an average $<\delta>/<I>$ value that is ~1.5x greater than that for microtubules ($p < 0.03$ using KS-Test described in Methods, Fig. 4). This result, which is in line with our previous findings for composites without crosslinkers[27], is not surprising given the ~100-fold lower bending rigidity of actin compared to microtubules. Comparing the mobility of the crosslinked composites to the unlinked composite (*None*), we find that all crosslinking motifs reduce the mobility of both filaments by ~1.4x ($p \leq 0.04$ and $p \leq 0.02$ for actin and microtubules, respectively). This result corroborates our relaxation data in which all three decay times for *None* are ~1.8x faster than for crosslinked composites (Fig. 3d). Likewise, the measured resistive force during strain for *None* is substantially smaller than for crosslinked composites, indicating it is more fluid and mobile (Fig. 2).

However, while we see a clear distinction in the force response of Class 1 and Class 2 composites at mesoscopic scales (and in the nonlinear regime) (Fig. 2), the mobilities of both actin and microtubules display minimal variation between the different crosslinking classes ($p > 0.09$ for actin, $p > 0.07$ for microtubules). Because the mobility we are measuring is at the submicron scale (each pixel is 0.41 μm) and in the steady-state (linear) regime, we expect our mobility results to more closely match our microrheology results at the submicron and microscopic scales (corresponding to the low-force, linear regime). As described above, at these lengths and force scales there
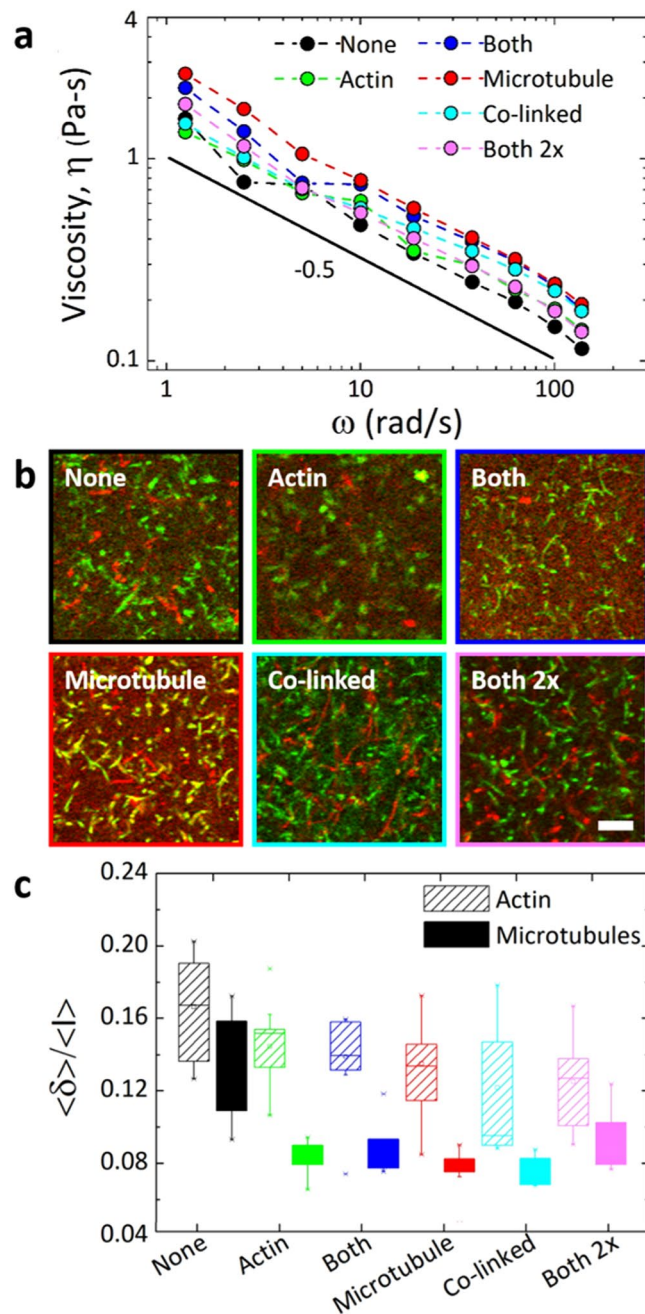
Figure 4. Differences between crosslinking motifs have minimal impact on the steady-state viscosity and filament mobility in actin-microtubule composites. (**a**) Complex viscosity $\eta(\omega)$ versus frequency ω for different crosslinking motifs displayed in legend. Solid line denotes power-law scaling with exponent shown. (**b**) For each composite, a 128×128 image shows the standard deviation of intensity values for each pixel over time for actin (green) and microtubules (red) in a 60 s time-series. Scale bar is $10\,\mu$m and applies to all images. (**c**) Box-whisker plot of the steady-state mobility, determined by computing the average standard deviation of pixel intensities $<\delta>$ normalized by the overall average pixel intensity $<I>$ for each time-series (as described in Methods). For each composite type, $<\delta>/<I>$ is calculated separately for actin (cross-hatched) and microtubules (solid) and each data point is computed from 10–12 time-series each collected in different regions of the sample chambers of two different samples. As shown, microtubules are less mobile than actin filaments in all composites. Further, while crosslinking reduces the mobility of both filaments, the specific crosslinking motif has little effect.

is little difference between the different crosslinking motifs, with all composites exhibiting similar force, stiffness and viscosity values (Fig. 2). This effect is also seen in the relaxation data in which the relaxation times for all crosslinked composites are similar.

Methods

Rabbit skeletal actin, biotinylated actin and Alexa-488-labeled actin were purchased from Cytoskeleton (AKL99, AB07) and Thermofisher (A12373) and stored at $-80\,°C$ in a Ca buffer (2 mM Tris (pH 8.0), 0.2 mM ATP, 0.5 mM DTT, 0.1 mM $CaCl_2$). Porcine brain tubulin, biotinylated tubulin, and rhodamine-labeled tubulin were purchased from Cytoskeleton (T240, T33P, TL590M) and stored at $-80\,°C$ in PEM-100 (100 mM PIPES (pH 6.8), 2 mM $MgCl_2$, and 2 mM EGTA).

Crosslinked networks were formed using preassembled biotin-NeutrAvidin complexes optimized previously for stable, isotropic crosslinking of actin networks[37]. As depicted in Fig. 1a, crosslinker complexes are comprised of NeutrAvidin flanked on either side by biotinylated actin and/or tubulin, depending on the desired crosslinking motif. We incorporated crosslinkers into previously established protocols to form co-entangled actin-microtubule composites[27]. In short, actin monomers, tubulin dimers, and crosslinker complexes were added to PEM-100 supplemented with 1 mM ATP, 1 mM GTP, and 5 μM Taxol. To image composites, 0.13 μM of Alexa-488-labeled actin filaments and rhodamine-labeled microtubules, as well as oxygen scavenging agents [4.5 mg/ml glucose, 0.5% β-mercaptoethanol, 4.3 mg/ml glucose oxidase, 0.7 mg/ml catalase] were added (Fig. 1b). To enable microrheology measurements, carboxylated microspheres (Polysciences, Inc.), with a 4.5 μm diameter, were also added (Fig. 1c). The solution was then mixed, pipetted into a ~20 μL sample chamber, and allowed to incubate at 37 °C for 30 minutes to co-polymerize both proteins.

We prepared six different composite types that varied in their crosslinking motif as follows (Fig. 1a): (1) no crosslinkers are present (*None*); (2) actin filaments in the composite are crosslinked to each other (*Actin*); (3) microtubules in the composite are crosslinked to each other (*Microtubule*); (4) both actin and microtubules are crosslinked but they cannot crosslink to each other (*Both*); (5) actin and microtubules are crosslinked to each other but not to themselves (*Co-linked*); and (6) a composite similar to *Both* but in which the densities of actin-actin and microtubule-microtubule crosslinks are both doubled (*Both 2x*).

For all presented data, total protein concentration was held fixed at 5.8 μM with an equimolar ratio of actin to tubulin, and the molar ratio of crosslinker to protein was fixed at $R = 0.02$. The mesh size of actin and microtubule networks comprising each composite are $\xi_a = 0.3/c_a^{1/2} = 0.85\,\mu$m and $\xi_m = 0.89/c_t^{1/2} = 1.58\,\mu$m in which c_a and c_t are the actin and tubulin concentrations in units of mg/ml[34,42,67]. From these mesh sizes we calculated the effective composite mesh as $\xi = (\xi_m^{-3} + \xi_a^{-3})^{-1/3} = 0.81\,\mu$m[27]. We estimated the length between crosslinkers for all three types of crosslinking used in composites (actin crosslinking, microtubule crosslinking, and actin-microtubule co-linking) as follows (Fig. 1a). The length between crosslinkers along an actin filament was determined by $l_{c,a} = \frac{1}{2}l_{mon} \times R^{-1}$ where $l_{mon} = 2.7$ nm is the length that each actin monomer adds to an actin filament. The ½ prefactor takes into account that each crosslinker is shared between two filaments. Similarly, the length between crosslinkers along a microtubule was calculated by $l_{c,m} = \frac{1}{2}(l_{ring}/13) \times R^{-1}$ where every 13 tubulin dimers adds $l_{ring} = 7.8$ nm in length to the microtubule. For *Actin* and *Microtubule* composites, $l_{c,a} = 67.5$ nm and $l_{c,m} = 15$ nm. In the composite where crosslinkers are equally distributed between actin-actin links and microtubule-microtubule links (*Both*), R remains fixed so there are half as many crosslinkers available to each network. Thus, $l_{c,a}$ and $l_{c,m}$ both double (i.e. $l_{c,a} = 135$ nm, $l_{c,m} = 30$ nm). For composites in which both networks are linked but R is doubled (*Both 2x*) $l_{c,a}$ and $l_{c,m}$ remain the same as in the *Actin* and *Microtubule* cases. For *Co-linked* composites, the length between crosslinkers that link actin to microtubules was computed as $l_{c,a-m} = (l_{c,a} \times l_{c,m})^{1/2} = 31$ nm.

The optical trap used in all microrheology measurements, which has been previously described and validated[27,36,37,68], was formed by a IX71 fluorescence microscope (Olympus) outfitted with a 1064 nm Nd:YAG fiber laser (Manlight) and focused with a 60× 1.4 NA objective (Olympus). A position-sensing detector (Pacific Silicon Sensor) measured the deflection of the trapping laser, which is proportional to the force acting on the trapped microsphere. Stokes drag method was used to calibrate trap stiffness[69,70]. A nanopositioning piezoelectric stage (Mad City Labs) was used to move the trapped microsphere relative the sample (Fig. 1c). Stage position and laser deflection were recorded at 20 kHz using custom-written Labview codes. The response time of the stage is 0.25 ms, so the data presented in Fig. 2 (strain phase) and Fig. 3 (relaxation phase) start at 2.5e-4 s when the stage has reached constant velocity (strain phase) or come to a complete stop (relaxation phase).

For the data presented in Figs 1–3, a trapped bead was displaced 10 μm at a constant speed of 10 μm/s relative to the sample chamber. The speed and displacement were chosen to ensure we were well within the nonlinear regime, which we previously showed to occur at ~3–5 μm/s[27]; and accessing mesoscopic scales, i.e. several times larger than ξ and comparable to the lengths of the filaments. We did not exceed this speed and displacement because for larger strain parameters the bead would not reliably stay trapped for the duration of the strain as the strength of the composite exceeded the strength of the trap. Oscillatory strain measurements (Fig. 4) were also performed in which the trapped sphere was sinusoidally displaced over an amplitude $A = 1\,\mu$m at frequencies $\omega = 1.26$–126 rad/s. From the amplitudes of the oscillatory force curves F_{max}, as well as the phase shift $\Delta\phi$ between the force and stage position curves we computed the complex viscosity, $\eta(\omega) = F_{max}(\omega)/3\pi Ad$ where d is the bead diameter (Fig. 4), as described previously[71].

Custom-written MATLAB scripts were used for post-measurement analysis. All displayed data are averages over 50–60 different trials taken between two samples. All trials were taken in different regions of the sample chamber, each separated by >100 μm.

A Nikon A1R laser scanning confocal microscope with a 60× 1.4 NA objective and QImaging QICAM CCD camera were used to collect 2D time-series of composites. The microscope is outfitted with 488 nm and 561 nm lasers and simultaneously records separate images for each laser channel (green and red) to separately visualize Alexa-488-actin (green) and rhodamine-tubulin (red) (Figs 1b, 4). Time-series of 512 × 512 images (0.41 μm/pixel) in each channel were recorded at 16 fps for 60 seconds. For each composite type, two different samples were imaged with 3–5 time-series taken for each sample.

Time-series from each channel (green and red) were analyzed separately to determine the mobility of actin and microtubules in the composites, as previously described[27]. In brief, every 16 frames in the time-series were

averaged together to create time-series with 1 second frames[27]. As demonstrated and described previously[27], we selected 1 second frames to average out the frame-to-frame shot noise that obscured the images of the filaments, enhancing the signal to noise without altering the trends in the data (Fig S3); and because the filaments do not significantly change position over that time (within the resolution of the measurement). From these averaged time-series, we used FIJI/ImageJ to create a single collapsed image for each channel that represented the standard deviation of each pixel over time (Fig. 4). The average standard deviation over all pixels was then calculated to give a single standard deviation value for the entire time-series $<\delta>$. This value, which represents the variation in intensity values for each pixel over time, is a measure of the extent to which filaments in the network fluctuate over time. To account for differences in overall intensity among different time-series, we also computed the average intensity over all pixels and frames for each time-series $<I>$, and normalized each standard deviation by this value. The resulting metric $<\delta>/<I>$, which quantifies the mobility of actin and microtubules in each time-series, is presented in Fig. 4. We carried out this analysis for all time-series collected for each composite type. We used the Kolmogorov-Smirnov statistical test (KS-Test, http://www.physics.csbsju.edu/stats/KS-test.html) to compare different data sets. From KS-tests, we computed probability values p for finding overlapping data and use the accepted value of $p < 0.05$ as the cutoff for determining when two data sets were significantly different.

Conclusion

Actin and microtubules form interacting networks within the cytoskeleton, providing cells with mechanical integrity and enabling a myriad of mechanical processes such as locomotion, morphogenesis, intracellular transportation, and division. Many of these diverse functions are mediated by crosslinking proteins that can bind actin, microtubules, or both proteins. Further, the role of crosslinking *between* actin and microtubules has received much recent attention and is thought to be responsible for maintaining cell shape and polarity, growth and structure of neurons, and spindle positioning in mitosis[8,15,16]. The design and characterization of composites of flexible and stiff polymers is also a topic of current interest in materials engineering[26,66], yet how crosslinking can tune the mechanical response of these composites has remained largely unexplored.

Here, we characterize the mobility and mechanics – from submicron to mesoscopic scales – of custom-designed composites of actin and microtubules with distinct crosslinking patterns. We create composites in which actin is crosslinked (*Actin*), microtubules are crosslinked (*Microtubule*), both actin and microtubules are crosslinked (*Both*), and actin and microtubules are crosslinked to each other (*Co-linked*). We use optical tweezers microrheology and dual-color fluorescence confocal microscopy to measure the nonlinear force response and mobility of each composite type. We show that composites separate into two distinct classes which are dictated by the degree to which microtubules in each composite are crosslinked. Class 1, which comprises *None*, *Actin*, and *Both* composites, displays largely viscoelastic response to the imposed strain with ample softening. In contrast, Class 2, comprised of *Microtubule*, *Co-linked* and *Both 2x* composites, elicit a substantially elastic response to perturbation. Notably, this distinction only emerges at mesoscopic scales in response to nonlinear forcing. Conversely, the crosslinking motif has little impact on the microscopic linear regime mechanics and steady-state filament mobility. These intriguing scale-dependent dynamics likely play a significant role in the ability of the composite cytoskeleton to mediate a vast array of different mechanical processes, and could be exploited to design multifunctional soft materials with scale-dependent mechanical properties. The custom-designed composites and measurement techniques demonstrated in this study further lay the groundwork for building complexity into *in vitro* cytoskeleton networks to determine how each component plays a role in cellular mechanics and in the design of novel biomimetic materials.

References

1. Huber, F., Boire, A., Lopez, M. P. & Koenderink, G. H. Cytoskeletal crosstalk: when three different personalities team up. *Current opinion in cell biology* **32**, 39–47 (2015).
2. Wen, Q. & Janmey, P. A. Polymer physics of the cytoskeleton. *Current Opinion in Solid State and Materials Science* **15**, 177–182 (2011).
3. Gittes, F., Mickey, B., Nettleton, J. & Howard, J. Flexural rigidity of microtubules and actin filaments measured from thermal fluctuations in shape. *The Journal of cell biology* **120**, 923–934 (1993).
4. Yang, Y., Bai, M., Klug, W. S., Levine, A. J. & Valentine, M. T. Microrheology of highly crosslinked microtubule networks is dominated by force-induced crosslinker unbinding. *Soft matter* **9**, 383–393 (2013).
5. Hawkins, T., Mirigian, M., Yasar, M. S. & Ross, J. L. Mechanics of microtubules. *Journal of biomechanics* **43**, 23–30 (2010).
6. Hawkins, T. L. *et al.* Perturbations in microtubule mechanics from tubulin preparation. *Cellular and Molecular. Bioengineering* **5**, 227–238 (2012).
7. Fuchs, E. & Karakesisoglou, I. Bridging cytoskeletal intersections. *Genes & development* **15**, 1–14 (2001).
8. Dogterom, M. & Koenderink, G. H. Actin–microtubule crosstalk in cell biology. *Nature Reviews Molecular Cell Biology*, **1** (2018).
9. Lopez, B. J. & Valentine, M. T. Molecular control of stress transmission in the microtubule cytoskeleton. *Biochimica et Biophysica Acta (BBA)-Molecular Cell Research* **1853**, 3015–3024 (2015).
10. Griffith, L. M. & Pollard, T. D. Evidence for actin filament-microtubule interaction mediated by microtubule-associated proteins. *The Journal of cell biology* **78**, 958–965 (1978).
11. Lin, Y.-C., Koenderink, G. H., MacKintosh, F. C. & Weitz, D. A. Control of non-linear elasticity in F-actin networks with microtubules. *Soft Matter* **7**, 902–906 (2011).
12. Kubitschke, H. *et al.* Actin and microtubule networks contribute differently to cell response for small and large strains. *New Journal of Physics* **19**, 093003 (2017).
13. Joo, E. E. & Yamada, K. M. Post-polymerization crosstalk between the actin cytoskeleton and microtubule network. *Bioarchitecture* **6**, 53–59 (2016).
14. Rodriguez, O. C. *et al.* Conserved microtubule–actin interactions in cell movement and morphogenesis. *Nature cell biology* **5**, 599 (2003).
15. Coles, C. H. & Bradke, F. Coordinating neuronal actin–microtubule dynamics. *Current Biology* **25**, R677–R691 (2015).
16. Fontela, Y. C. *et al.* Multivalent cross-linking of actin filaments and microtubules through the microtubule-associated protein Tau. *Nature communications* **8**, 1981 (2017).
17. Wiche, G. Role of plectin in cytoskeleton organization and dynamics. *Journal of cell science* **111**, 2477–2486 (1998).

18. Applewhite, D. A. *et al*. The spectraplakin short stop is an actin–microtubule cross-linker that contributes to organization of the microtubule network. *Molecular biology of the cell* **21**, 1714–1724 (2010).

19. Henty-Ridilla, J. L., Rankova, A., Eskin, J. A., Kenny, K. & Goode, B. L. Accelerated actin filament polymerization from microtubule plus ends. *Science* **352**, 1004–1009 (2016).

20. Henty-Ridilla, J. L., Juanes, M. A. & Goode, B. L. Profilin Directly Promotes Microtubule Growth through Residues Mutated in Amyotrophic Lateral Sclerosis. *Current Biology* **27**, 3535–3543. e3534 (2017).

21. Juanes, M. A. *et al*. Adenomatous polyposis coli nucleates actin assembly to drive cell migration and microtubule-induced focal adhesion turnover. *J Cell Biol, jcb*. 201702007 (2017).

22. Mandato, C. A. & Bement, W. M. Actomyosin transports microtubules and microtubules control actomyosin recruitment during Xenopus oocyte wound healing. *Current Biology* **13**, 1096–1105 (2003).

23. Schaefer, A. W., Kabir, N. & Forscher, P. Filopodia and actin arcs guide the assembly and transport of two populations of microtubules with unique dynamic parameters in neuronal growth cones. *The Journal of cell biology* **158**, 139–152 (2002).

24. Hirokawa, N. Cross-linker system between neurofilaments, microtubules and membranous organelles in frog axons revealed by the quick-freeze, deep-etching method. *The Journal of cell biology* **94**, 129–142 (1982).

25. Salmon, W. C., Adams, M. C. & Waterman-Storer, C. M. Dual-wavelength fluorescent speckle microscopy reveals coupling of microtubule and actin movements in migrating cells. *The Journal of cell biology* **158**, 31–37 (2002).

26. Das, M. & MacKintosh, F. Mechanics of soft composites of rods in elastic gels. *Physical Review E* **84**, 061906 (2011).

27. Ricketts, S. N., Ross, J. L. & Robertson-Anderson, R. M. Co-Entangled Actin-Microtubule Composites Exhibit Tunable Stiffness and Power-Law Stress Relaxation. *Biophysical journal* **115**, 1055–1067 (2018).

28. Ajayan, P. M. & Tour, J. M. Materials science: nanotube composites. *Nature* **447**, 1066 (2007).

29. Al-Saleh, M. H. & Sundararaj, U. Review of the mechanical properties of carbon nanofiber/polymer composites. *Composites Part A: Applied Science and Manufacturing* **42**, 2126–2142 (2011).

30. Chen, Q., Chen, H., Zhu, L. & Zheng, J. Fundamentals of double network hydrogels. *Journal of Materials Chemistry B* **3**, 3654–3676 (2015).

31. Gong, J. P. Why are double network hydrogels so tough? *Soft Matter* **6**, 2583–2590 (2010).

32. Sun, J.-Y. *et al*. Highly stretchable and tough hydrogels. *Nature* **489**, 133 (2012).

33. Hu, J. *et al*. Microgel-reinforced hydrogel films with high mechanical strength and their visible mesoscale fracture structure. *Macromolecules* **44**, 7775–7781 (2011).

34. Gardel, M., Valentine, M., Crocker, J. C., Bausch, A. & Weitz, D. Microrheology of entangled F-actin solutions. *Physical review letters* **91**, 158302 (2003).

35. Gardel, M. *et al*. Prestressed F-actin networks cross-linked by hinged filamins replicate mechanical properties of cells. *Proceedings of the National Academy of Sciences* **103**, 1762–1767 (2006).

36. Gurmessa, B., Fitzpatrick, R., Falzone, T. T. & Robertson-Anderson, R. M. Entanglement density tunes microscale nonlinear response of entangled Actin. *Macromolecules* **49**, 3948–3955 (2016).

37. Gurmessa, B., Ricketts, S. & Robertson-Anderson, R. M. Nonlinear Actin Deformations Lead to Network Stiffening, Yielding, and Nonuniform Stress Propagation. *Biophysical Journal* (2017).

38. Hinner, B., Tempel, M., Sackmann, E., Kroy, K. & Frey, E. Entanglement, elasticity, and viscous relaxation of actin solutions. *Physical Review Letters* **81**, 2614 (1998).

39. Isambert, H. & Maggs, A. Dynamics and rheology of actin solutions. *Macromolecules* **29**, 1036–1040 (1996).

40. Lee, H., Ferrer, J. M., Nakamura, F., Lang, M. J. & Kamm, R. D. Passive and active microrheology for cross-linked F-actin networks in vitro. *Acta biomaterialia* **6**, 1207–1218 (2010).

41. Lieleg, O., Schmoller, K., Claessens, M. M. & Bausch, A. Cytoskeletal polymer networks: viscoelastic properties are determined by the microscopic interaction potential of cross-links. *Biophysical journal* **96**, 4725–4732 (2009).

42. Lin, Y.-C., Koenderink, G. H., MacKintosh, F. C. & Weitz, D. A. Viscoelastic properties of microtubule networks. *Macromolecules* **40**, 7714–7720 (2007).

43. Liu, J., Koenderink, G., Kasza, K., MacKintosh, F. & Weitz, D. Visualizing the strain field in semiflexible polymer networks: strain fluctuations and nonlinear rheology of F-actin gels. *Physical review letters* **98**, 198304 (2007).

44. Luan, Y., Lieleg, O., Wagner, B. & Bausch, A. R. Micro-and macrorheological properties of isotropically cross-linked actin networks. *Biophysical journal* **94**, 688–693 (2008).

45. Müller, K. W. *et al*. Rheology of semiflexible bundle networks with transient linkers. *Physical review letters* **112**, 238102 (2014).

46. Xu, J., Wirtz, D. & Pollard, T. D. Dynamic cross-linking by α-actinin determines the mechanical properties of actin filament networks. *Journal of Biological Chemistry* **273**, 9570–9576 (1998).

47. Yang, Y. & Valentine, M. T. In *Methods in cell biology* Vol. 115, 75–96 (Elsevier, 2013).

48. Falzone, T. T. & Robertson-Anderson, R. M. Active entanglement-tracking microrheology directly couples macromolecular deformations to nonlinear microscale force response of entangled actin. *ACS Macro Letters* **4**, 1194–1199 (2015).

49. Wang, S.-Q. *et al*. New experiments for improved theoretical description of nonlinear rheology of entangled polymers. *Macromolecules* **46**, 3147–3159 (2013).

50. Head, D. A., Levine, A. J. & MacKintosh, F. Deformation of cross-linked semiflexible polymer networks. *Physical review letters* **91**, 108102 (2003).

51. Doi, M. & Edwards, S. F. *The theory of polymer dynamics*. Vol. 73 (oxford university press, 1988).

52. De Gennes, P.-G. *Scaling concepts in polymer physics*. (Cornell university press, 1979).

53. Kim, T., Gardel, M. L. & Munro, E. Determinants of fluidlike behavior and effective viscosity in cross-linked actin networks. *Biophysical journal* **106**, 526–534 (2014).

54. Žagar, G., Onck, P. R. & van der Giessen, E. Two fundamental mechanisms govern the stiffening of cross-linked networks. *Biophysical journal* **108**, 1470–1479 (2015).

55. Åström, J. A., Kumar, P. S., Vattulainen, I. & Karttunen, M. Strain hardening, avalanches, and strain softening in dense cross-linked actin networks. *Physical Review E* **77**, 051913 (2008).

56. Yang, Y., Lin, J., Meschewski, R., Watson, E. & Valentine, M. T. Portable magnetic tweezers device enables visualization of the three-dimensional microscale deformation of soft biological materials. *BioTechniques* **51**, 29–34 (2011).

57. Regan, K., Wulstein, D., Rasmussen, H., McGorty, R. & Robertson-Anderson, R. M. Bridging the spatiotemporal scales of macromolecular transport in crowded biomimetic systems. *Soft matter* (2019).

58. Pelletier, V., Gal, N., Fournier, P. & Kilfoil, M. L. Microrheology of microtubule solutions and actin-microtubule composite networks. *Physical review letters* **102**, 188303 (2009).

59. Das, M., Quint, D. & Schwarz, J. Redundancy and cooperativity in the mechanics of compositely crosslinked filamentous networks. *PloS one* **7**, e35939 (2012).

60. Tharmann, R., Claessens, M. & Bausch, A. Viscoelasticity of isotropically cross-linked actin networks. *Physical review letters* **98**, 088103 (2007).

61. Bell, G. I. Models for the specific adhesion of cells to cells. *Science* **200**, 618–627 (1978).

62. Ferrer, J. M. *et al*. Measuring molecular rupture forces between single actin filaments and actin-binding proteins. *Proceedings of the National Academy of Sciences* **105**, 9221–9226 (2008).

63. Falzone, T. T., Blair, S. & Robertson-Anderson, R. M. Entangled F-actin displays a unique crossover to microscale nonlinearity dominated by entanglement segment dynamics. *Soft matter* **11**, 4418–4423 (2015).
64. Käs, J., Strey, H. & Sackmann, E. Direct imaging of reptation for semiflexible actin filaments. *Nature* **368**, 226 (1994).
65. Mickey, B. & Howard, J. Rigidity of microtubules is increased by stabilizing agents. *The Journal of cell biology* **130**, 909–917 (1995).
66. Bausch, A. & Kroy, K. A bottom-up approach to cell mechanics. *Nature physics* **2**, 231 (2006).
67. Schmidt, C. F., Baermann, M., Isenberg, G. & Sackmann, E. Chain dynamics, mesh size, and diffusive transport in networks of polymerized actin: a quasielastic light scattering and microfluorescence study. *Macromolecules* **22**, 3638–3649 (1989).
68. Robertson-Anderson, R. M. Optical Tweezers Microrheology: From the Basics to Advanced Techniques and Applications, ACS Macro Letters. https://doi.org/10.1021/acsmacrolett.8b00498 (ACS Publications, 2018).
69. Williams, M. C. Optical tweezers: measuring piconewton forces. *Biophysics Textbook Online*: http://www. biophysics.org/btol (2002).
70. Brau, R. *et al*. Passive and active microrheology with optical tweezers. *Journal of Optics A: Pure and Applied Optics* **9**, S103 (2007).
71. Chapman, C. D., Lee, K., Henze, D., Smith, D. E. & Robertson-Anderson, R. M. Onset of Non-Continuum Effects in Microrheology of Entangled Polymer Solutions. *Macromolecules* **47**, 1181–1186, https://doi.org/10.1021/ma401615m (2014).

Author Contributions

S.N.R. designed and conducted microscopy and optical tweezer experiments, analyzed and interpreted data, and wrote the manuscript; M.L.F. conducted optical tweezer experiments and analyzed data; L.F. analyzed and interpreted microscopy data; M.J.R. helped analyze and interpret data; M.D. helped interpret data and write the manuscript; J.L.R. analyzed and interpreted data and helped write the manuscript; R.M.R.-A. designed and advised experiments, analyzed and interpreted data, and wrote the manuscript.

Additional Information

Supplementary information accompanies this paper at https://doi.org/10.1038/s41598-019-49236-4.

Competing Interests: The authors declare no competing interests.

Publisher's note: Springer Nature remains neutral with regard to jurisdictional claims in published maps and institutional affiliations.